Evaluation and Correction of Viewing Angle Effects on Satellite Measurements of Bidirectional Reflectance

Alain Royer
Pierre Vincent
Ferdinand Bonn
Centre d'Applications et de Recherches en Télédétection (CARTEL),
Université de Sherbrooke, Sherbrooke, Québec J1K 2R1, Canada

ABSTRACT: The effects of the angular anisotropy of reflective properties of natural surfaces are studied with an airborne multispectral scanner, which allows us to analyze the radiance variations with respect to viewing angle for its ± 37° scan angle range and under different illumination conditions. With respect to seven cover-types, the off-nadir effects are significant (mean relative variation of 60 percent) and are asymmetric about the nadir. They are accentuated with increasing solar zenith angle and are maximized when the scan direction is parallel to the incoming solar radiation. The computed bidirectional reflectance distribution functions are characteristic of each type of canopy and show that the separability or spatial contrast between cover-types can be increased in oblique mode measurements. Original and simple practical correction methods, based on normalization of the measured radiances using quadratic regression curves of the reflectance variation functions, are tested. The correction procedures significantly remove the radiometric inhomogeneity in images recorded with wide scan angles and allow direct comparison of images recorded in vertical and oblique modes.

INTRODUCTION

THE REFLECTIVE PROPERTIES of vegetative materials are influenced to a great extent both by ground illumination conditions and by atmospheric factors related to viewing angle geometry. To compare measurements performed under different geometric and illumination conditions, one must take into account atmospheric effects as well as the angular anisotropy of the reflective properties of natural surfaces. The non-Lambertian assumption for satellite measurements of ground reflectance has been studied extensively, particularly for vegetative surfaces (e.g., Kriebel, 1978; Eaton and Dirmhin, 1979; Smith *et al.*, 1980; Guyot, 1980; Kimes *et al.*, 1984).

Spectral reflectance is influenced by a large number of variables, including crop type and texture (Vanderbilt, 1981), plant and crop geometry (Rao *et al.*, 1979), illumination conditions (solar zenith and azimuth angles) (Duggin, 1977; Jackson *et al.*, 1979; Kimes *et al.*, 1980), and viewing geometry (viewing zenith and azimuth angles) (Staenz *et al.*, 1981; D'Arodes *et al.*, 1983; Holben and Fraser, 1983). Measurements from space are also perturbed by atmospheric effects, including aerosol and molecular backscattering (Turner and Spencer, 1972; Tanré *et al.*, 1979), and the angular dependence of the atmospheric reflectance must be substracted from the measurements (Tanré *et al.*, 1983). For non-uniform sites, the reflectance for a given point is altered by the contribution of the target background (Kaufman and Fraser, 1983; Dave, 1980; Tanré *et al.*, 1981). The bidirectional properties of the target reflectance are partially smoothed over by atmospheric scattering processes, which are dependent upon atmospheric conditions and geometrical factors.

However, little consideration has been given to the implications of wide viewing angle effects for standard image processing techniques. Most studies are limited to either ground measurement of bidirectional reflectance or satellite measurement over rugged terrain. Moreover, the variations of atmospheric reflectance with viewing angle are usually neglected.

Corrections for illumination and viewing geometry effects will become very important as new satellites with wide scan angles and with off-nadir viewing geometry are introduced. This is particularly the case for the ±56° scan angle range of the Advanced Very High Resolution Radiometer on NOAA satellites (Brown *et al.*, 1982; Piwinsky *et al.*, 1983). The off-track viewing geometry with the Haute Résolution Visible (HRV) sensor on the SPOT satellite (Chevrel *et al.*, 1981) and the Multispectral Resources Sampler (Slater, 1980) will affect the apparent spectral reflectance properties of targets.

PHOTOGRAMMETRIC ENGINEERING AND REMOTE SENSING,
Vol. 51, No. 12, December 1985, pp. 1899-1914.

0099-1112/85/5112-1899$02.25/0

Airborne multispectral scanners, such as the Daedalus with a scan angle of 70°, are also seriously affected by off-nadir view angle effects.

All these perturbations will make the quantitative interpretation of the data invalid as well as render impossible digital classification over a whole image, and they will affect the results of multitemporal studies.

This paper presents a practical analysis of the implications of view angle effects on image processing techniques currently employed in vegetation studies. Specifically, the purpose of our investigation is to analyze angular bidirectional reflectance variations from airborne data, and to test simple empirical correction methods based on the normalization of the measured radiances using a quadratic regression curve of the reflectance variation function. First, we present the data and an evaluation of the off-nadir viewing angle effects. We then assess the efficiency of the correction procedures.

DATA COLLECTION

The experimental spectral measurements were obtained with the Daedalus DS-1260 airborne multi-spectral scanner of the Canada Centre for Remote Sensing (CCRS) (Zwick *et al.*, 1980) (Table 1). The measurements were made in seven spectral bands in the visible and the near-infrared wavelengths (Table 2). Daedalus bands 3, 5, 7, and 9 correspond closely to the first four channels of the Thematic Mapper sensor aboard Landsat-5. The Daedalus has a scan angle of ±37° from nadir, which allows us to measure a large number of training areas under different viewing angles.

The overflights were conducted on 15 and 18 August 1982 near Huntingdon (Figure 1) and Sherbrooke, Québec, Canada, over flat terrain. Five low altitude flights (labeled F1 to F5) were flown with different track azimuth angles and under different solar elevation angles (Table 1).

Figure 2 shows geometrical relationships between the sun, the scan sensor plane, and the target. Because each flight line of data was recorded during a relatively short time (about 5 minutes), we assume a constant solar zenith angle for all the samples within the scanned image during the overflight. The sensor azimuth angle is constant along the image assuming a linear flight path of the aircraft. Over flat terrain, we can use a single relative azimuth angle between the incident and observation planes: $\emptyset = |\emptyset_s - \emptyset_v|$, where $\emptyset_s$ and $\emptyset_v$ are the solar and viewing azimuth angles, respectively. The directional reflectance $[\rho(\theta_s,\theta_v,\emptyset)]$ is a function of θ_s and θ_v, the solar and viewing zenith angles, and of $\emptyset$, the relative azimuth angle (Figure 2).

An understanding of the influence of each of the illumination and geometry effects is best achieved by allowing one variable to vary while the others are held constant. In these experiments θ_s and $\emptyset$ are constant, while the sensor zenith angle θ_v varies for all the targets in the same image. Θ_v is determined by the position of the individual target within the image and, hence, is related to the pixel coordinate.

Flights F1, F2, and F3 were used to analyze the bidirectional reflectance variances, while flights F4 and F5 were used for testing the correction methods. Flights F1 and F4 have parallel paths such that the swaths have a 50 percent overlap. Flights F2 and F5 have the same overlap but have different solar zenith and azimuth angles compared to flights F1 and F4 (Table 1).

Four major types of covers of agricultural importance were selected within the study areas for extensive analysis: corn, alfalfa, grass hay, and green pasture. Three other targets were chosen as references: water, asphalt road, and bare soil. All the test sites are homogeneous with respect to the spatial resolution of the image (pixel size of approximately 10 by 10 metres). For each surface type, eight to 15 targets with 50 to 100 pixels per sampling site were selected across the full swath width. Terrain slopes are generally less than 10 percent. Ground investigations were conducted to obtain all textural and landform information on the studied crops (Vincent *et al.*, 1983).

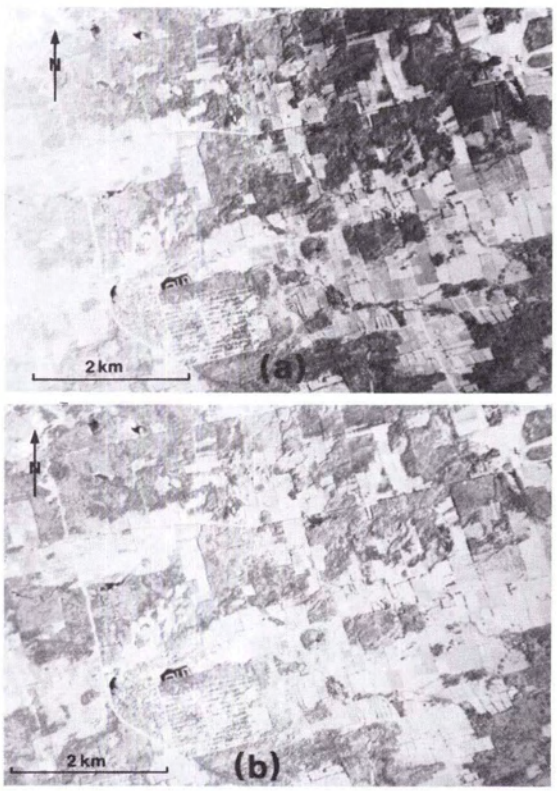

FIG. 1. Comparison between (a), the raw image, and (b), the corrected image with correction procedure 2, for flight line F1 at the Huntingdon site.

TABLE 1. ILLUMINATION CONDITIONS AND VIEWING GEOMETRY OF THE FIVE FLIGHT LINES (ALL ANGLES ARE EXPRESSED IN DEGREES). N.S., S.N., AND E.W. INDICATE THE APPROXIMATE DIRECTION OF THE FLIGHT LINES: NORTH TO SOUTH, SOUTH TO NORTH, AND EAST TO WEST, RESPECTIVELY

Flight Lines	Date	Hour (G.M.T.)	Altitude (km)	Spatial resolution (m)	Solar zenith angle	Solar azimuth angle	Viewing zenith angle	Viewing azimuth angle	Relative azimuth angle
Huntingdon N.S.: F1	82-08-15	14:18	4.51	11.9 × 9.4	45.3	140	−37 – +37	285	145
Sherbrooke N.S.: F2	82-08-18	13:36	4.57	12.6 × 9.6	52.0	129	−37 – +37	274	145
Cookshire E.W.: F3	82-08-18	13:20	4.57	12.6 × 9.6	54.5	125	−37 – +37	18	107
Huntingdon N.S.: F4	82-08-15	14:39	4.51	12.3 × 9.4	42.5	145	−37 – +37	285	145
Sherbrooke S.N.: F5	82-08-18	13:28	4.57	12.6 × 9.6	52.5	128	−37 – +37	268	140

TABLE 2. WAVEBANDS AND CENTRAL WAVELENGTHS ($\bar{\lambda}$) OF THE SEVEN DAEDALUS MSS BANDS USED AND THE CORRESPONDING ESTIMATED ATMOSPHERIC PARAMETERS (τ AND ρ_a) FOR THE FIRST THREE FLIGHTS

Flights			F1		F2		F3	
# channel	Wavebands (μm) $\Delta\lambda$	$\bar{\lambda}$	Optical depth	Nadir atmospheric reflectance	Optical depth	Nadir atmospheric reflectance	Optical depth	Nadir atmospheric reflectance
3	0.445 – 0.495	0.47	0.238	0.0365	0.303	0.0432	0.303	0.0465
4	0.500 – 0.550	0.52	0.191	0.0246	0.249	0.0300	0.249	0.0322
5	0.550 – 0.595	0.57	0.170	0.0197	0.223	0.0245	0.223	0.0262
6	0.590 – 0.645	0.62	0.149	0.0154	0.198	0.0197	0.198	0.0210
7	0.625 – 0.695	0.67	0.136	0.0142	0.183	0.0189	0.183	0.0202
8	0.680 – 0.780	0.74	0.119	0.0111	0.161	0.0153	0.161	0.0163
9	0.765 – 0.895	0.84	0.102	0.0085	0.139	0.0121	0.139	0.0129
	visibility (km)			30		25		25

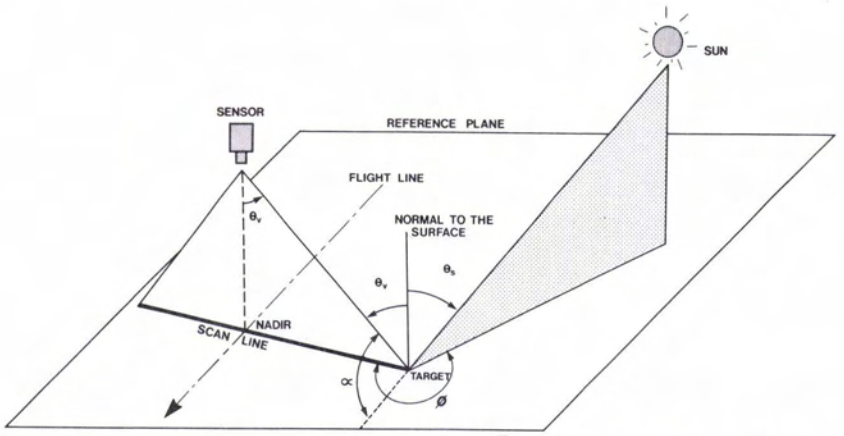

FIG. 2. Geometric relationships between sun, target, and sensor positions.

RADIOMETRIC CORRECTIONS

The digital counts in each channel were converted into apparent radiances using the calibration factors of the CCRS Daedalus 1260 (McColl, 1982). The atmospheric parameters were deduced from the nadir atmospheric path radiance. The nadir atmospheric path radiance, in turn, is estimated from the measured clear water radiances using the scattergram method suggested by Piech and Schott (1974). The atomospheric optical depth, expressed as the visibility V (in kilometres), was inferred from the nadir path radiance observations with the radiative transfer model of Deschamps *et al.* (1981). Table 2 gives the corresponding atmospheric parameters for flights F1, F2, and F3.

EXPERIMENTAL RESULTS

VIEWING ANGLE EFFECTS

In order to examine the implication of viewing angle effects on radiance measurements, the mean detected spectral radiances of the individual cover-types are plotted as a function of viewing angle for flight F1, F2, and F3 conditions (Figures 3, 4, and 5), and for the red and near infrared wavebands (channels 5 and 9, respectively). These radiances include atmospheric effects. The results indicate

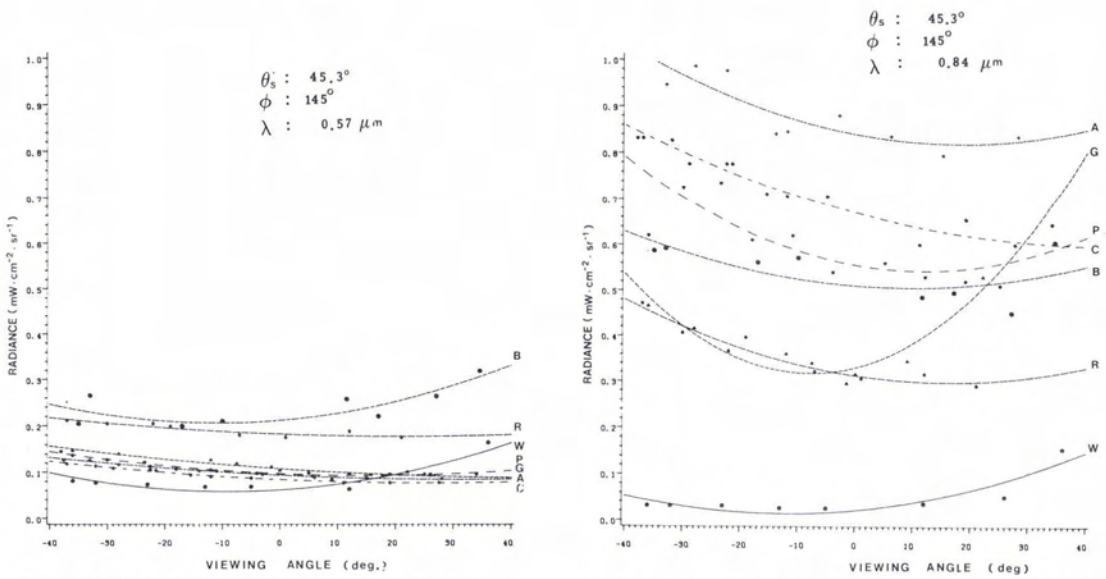

FIG. 3. Variation of the measured radiance with viewing angle for seven cover-types and two wavebands from the F1 data set. The curves correspond to the regression quadratic fit. A (+———): alfalfa, B (○———): bare soil, C (◆———): corn, G (▲———): grass, P (*———): pasture, R (★———): road, W (○———): water.

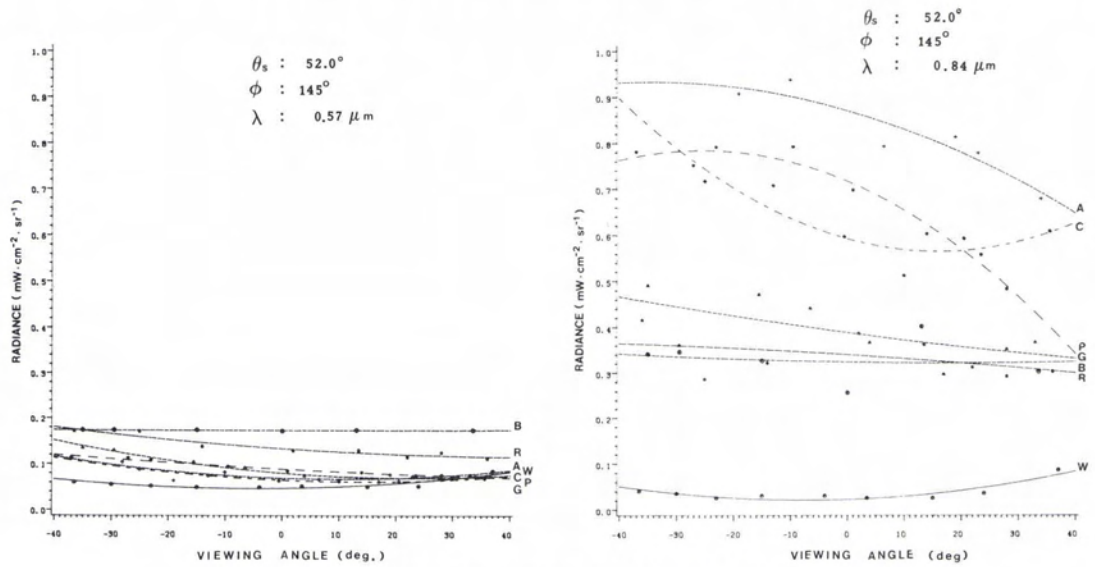

FIG. 4. Same as Figure 2 but for the F2 data set.

that, in general, there is an increase in radiance values with increasing off-nadir viewing angle away from the sun (Figure 1), and, with certain cover types, a decrease when viewing toward the sun. In almost all the cases, the off-nadir effects are significant and asymmetric about the nadir. The variations are characterized very well by regression curves of the form $L(\Theta_v) = a + b\Theta_v + c\Theta_v^2$ with determination coefficients (R^2) of 0.7, typically, or greater. Table 3 shows the R^2 values corresponding to the curves plotted in Figure 3, 4, and 5. For some cases (at 0.84 μm, for example), the variability of the measured radiances gives some lower R^2 values.

The amplitude of the off-nadir effects has been estimated for each surface, each wavelength, and each over-flight by computing the observed scan-angle contrast. This is defined as the relative increase between the minimum and the maximum detected spectral responses which occurred within the scan angle range. The scan-angle contrast of the radiances varies significantly between the different cover types (Table 4). Three groups of angular anisotropy can be distinguished. The first group consists of the vegetative surfaces characterized by an antispecular (hot spot) reflection mode which results from the backscattering process. The radiances

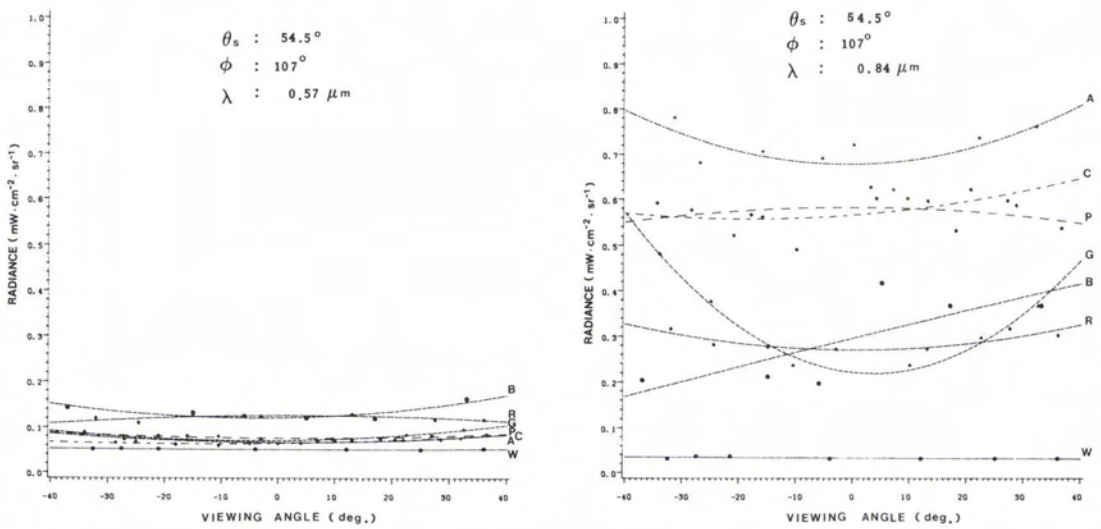

FIG. 5. Same as Figure 2 but for the F3 data set.

TABLE 3. DETERMINATION COEFFICIENT (R^2) OF THE MEASURED RADIANCES AS A FUNCTION OF VIEWING ANGLE FOR TWO WAVELENGTHS AND FOR THREE ILLUMINATION GEOMETRIES (SEE TABLE 1)

Flights	F1		F2		F3	
λ (μm)	0.57	0.84	0.57	0.84	0.57	0.84
Grass	0.87	0.88	0.65	0.98	0.97	0.43
Corn	0.99	0.93	0.79	0.28	0.99	0.76
Pasture	0.97	0.67	0.77	0.07	0.97	0.97
Asphalt Road	0.83	0.94	0.39	0.70	0.91	0.21

increase when viewing away from the sun (Θ_v denoted $-$) by a factor of about 50 to 80 percent, and decrease when viewing toward the sun (Θ_v denoted $+$). The second group is the result of a forward-scatter or specular reflection mode. Such a variation is typical of bare soil (summer fallow, sand and gravel pits) or water radiance variations. The third group consists of the approximately diffuse or Lambertian surface of asphalt roads. The radiance variations are lower and quasi-linear, in accordance with the measurements by Egbert and Ulaby (1972) of a similar surface.

ILLUMINATION CONDITION EFFECTS

The solar zenith angle effects on the radiance scan-angle variations are shown through the comparison between flights F1 and F2 (Figures 3 and 4). Flights F1 and F2 have approximately the same relative azimuth angle $\emptyset$, but have different solar zenith angles (Table 1). Table 5 shows some examples of the magnitude of the scan angle contrast for four cover-types. It can be seen that the recorded scan-angle variations depend highly on solar zenith angle. However, it should be noted that the atmospheric effects and the test sites are different for flights F1 and F2. The scan-angle contrasts increase with sun angle due to the greater difference between backward and forward scattering. A mean increase of 60 percent is found between the two profiles considered for the grass cover type (Table 5). The reverse situation was found for the water surface characterized by a specular mode (Table 5).

It appears that in such examples it is necessary to be aware of the sun angle effects on the off-nadir radiance profiles.

The effects of the relative azimuth angle between the sun and the sensor on the radiance scan variation are shown through the comparison of flights F2 and F3. Flights F2 and F3 have the same solar zenith angle while their respective relative azimuth angles are significantly different (Table 1). The radiance variations induced by off-nadir viewing are maximized when the scan direction is nearly parallel to the incoming solar radiation (Figure 4). Such a geometry occurs for the illumination condition of flight F2 ($\emptyset$ = 145°) (Table 6). A scan direction perpendicular to the incoming solar radiation minimizes the changes in radiances with viewing angle (F3: $\emptyset$ = 107°, Figure 5). This is explained by the smaller percentage of shadowed areas observed when viewing off-nadir toward the sun.

WAVELENGTH DEPENDENCE

Figure 6 shows the wavelength dependence of radiance variations for green pasture and corn. The scan-angle perturbation decreases with increasing wavelength. The lowest values of the scan-angle contrast can be seen in the red wavebands (0.625 μm to 0.695 μm and 0.680 μm to 0.780 μm). An increasing scan-angle contrast can then be found at 0.84 μm (Table 4). In general, the surface reflection properties show two significantly different behaviors for the visible and near-infrared (IR) wavebands (Figure 6). The wavelength dependence of viewing angle effects is in part due to atmospheric effects.

TABLE 4. SCAN ANGLE CONTRAST IN PERCENT OF DIFFERENT COVER-TYPE RADIANCES FOR DIFFERENT WAVELENGTHS, DEDUCED FROM F1 DATA (θ_s = 45.3° AND ϕ = 145°)

λ (μm)	0.47	0.52	0.57	0.62	0.67	0.74	0.84
Grass	78	70	73	79	67	68	57
Alfalfa	67	46	48	55	14	13	28
Corn	63	55	55	54	29	20	38
Pasture	72	58	53	51	27	42	63
Bare Soil	32	50	60	81	52	33	25
Asphalt Road	28	25	21	17	23	44	62
Water	108	134	160	216	274	333	500

TABLE 5. SCAN ANGLE CONTRAST IN PERCENT OF DIFFERENT COVER-TYPE RADIANCES FOR TWO SOLAR ZENITH ANGLES AND FOR FOUR WAVELENGTHS

λ (μm)	0.47		0.57		0.67		0.84	
Solar zenith angle (deg.)	45.3	52.0	45.3	52.0	45.3	52.0	45.3	52.0
Grass	78	125	73	143	67	118	57	66
Corn	63	62	55	42	29	22	38	40
Pasture	72	81	53	53	27	28	63	62
Asphalt Road	28	70	21	54	23	41	62	43

ATMOSPHERIC EFFECTS

The angular anisotropy of recorded radiance is also affected by atmospheric turbidity. We have simulated the angular dependence of the atmospheric reflectance for three different scattering atmospheric conditions (Visibility: V15, V23, V30), computed with the LOA model as described by Deschamps *et al.* (1981) (Figure 7). Simulations were calculated with the same illumination and geometry conditions as for flight F1 (Table 1). The calculations reveal a significant increase in the intrinsic atmospheric reflectance with increasing off-nadir viewing angle away from the sun (θ_v denoted $-$) (Figure 7). The inflection of the backscatter curve can be attributed in part to Rayleigh scattering, which is strongest for shorter wavelengths. Under the optimum measurement conditions (V30, Table 2) for which we have the best fit between the estimated and simulated nadir atmospheric reflectance, the computed relative scan-angle contrasts are 96, 102, 100, and 109 percent, respectively, for each wavelength. Under poor measurement conditions (V15: $\tau(\lambda = 0.57\ \mu m) = 0.40$ at nadir), the corresponding scan-angle contrast is found to be higher: i.e., 107, 118, 113, and 120 percent, respectively. The variations under standard measurement conditions (V23) appear to be the intermediate case. Clearly, the amplitude of the atmospheric reflectance exhibits large directional effects which are comparable with the ground effects.

In Figure 7, we have also plotted the estimated atmospheric reflectance variation as a function of viewing angle deduced from the observed variations of clear water radiances. This practical approach gives a maximum error of 20, 22, 36, and 76 percent for each wavelength when $\theta_v = 30°$. For the near IR waveband, the estimated atmospheric reflectance was considered as constant with viewing angle. In spite of the discrepancy between the two curves for the highest viewing angles, the estimated directional reflectance distribution function of clear water is a good approximation of the atmospheric directional effects for θ_v less than 30°.

Using these estimated atmospheric optical depths (τ) and atmospheric reflectances (Table 2), the spectral bidirectional reflectance function $\rho(\theta_s,\theta_v,\phi)$ can then be computed according to

$$\rho(\theta_s,\theta_v,\phi) = \frac{[\rho^*(\theta_s,\theta_v,\phi) - \rho_a(\tau,\theta_s,\theta_v,\phi)]}{T_s(\tau,\theta_s).T_v(\tau,\theta_v) + s(\tau)\,[\rho^*(\theta_s,\theta_v,\phi) - \rho_a(\tau,\theta_s,\theta_v,\phi)]} \quad (1)$$

where $\rho^*(\theta_s,\theta_v,\phi)$ is the apparent reflectance in the viewing direction (θ_v,ϕ_v) when the ground is illuminated by the solar incident beam in the direction (θ_s,ϕ_s);
$\rho_a(\tau,\theta_s,\theta_v,\phi)$ is the intrinsic atmospheric reflectance;
$T_s(\tau,\theta_s)$ and $T_v(\tau,\theta_v)$ are the total (direct plus scattered) downward and upward attenuation coefficients, respectively; and
$s(\tau)$ is the atomospheric spherical albedo which does not depend on the geometric parameters.

Knowledge of the angular dependence of the intrinsic atmospheric reflectance greatly increases the possibility of detecting ground directional contrast. To evaluate the pertubation due to atmospheric ef-

TABLE 6. SCAN ANGLE CONTRAST IN PERCENT OF DIFFERENT COVER-TYPE RADIANCES FOR TWO RELATIVE AZIMUTH ANGLES AND FOR FOUR WAVELENGTHS

λ (μm)	0.47		0.57		0.67		0.84	
Relative azimuth angle (deg.)	145	107	145	107	145	107	145	107
Grass	125	32	143	41	118	68	66	104
Corn	62	21	42	23	22	46	40	26
Pasture	81	25	53	13	28	31	62	20
Asphalt Road	70	19	54	18	41	25	43	17

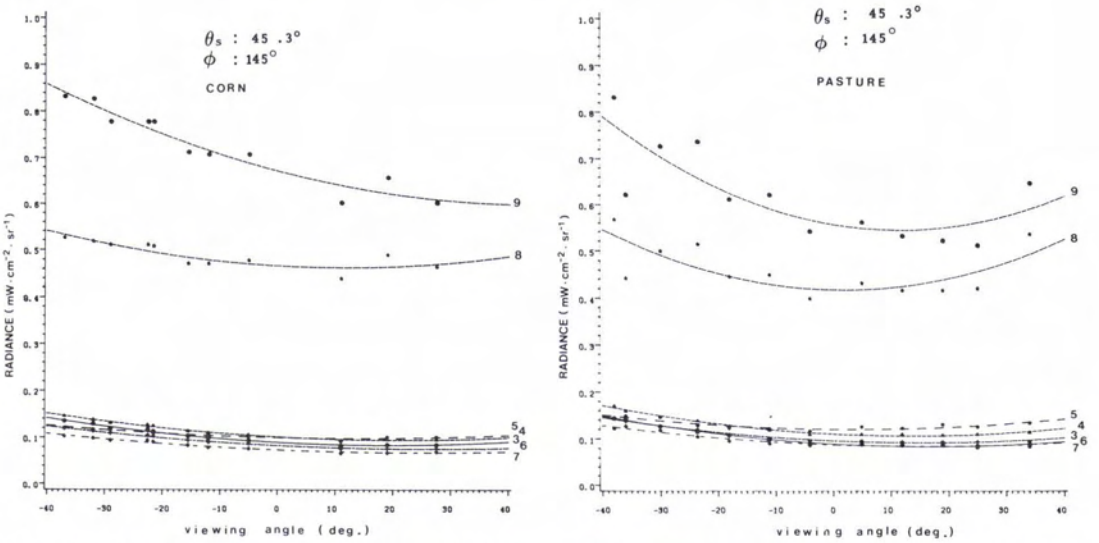

FIG. 6. Variation of the measured radiance with viewing angle for seven wavebands and for two cover-types. The curves correspond to the regression quadratic fit. The numbers refer to the channel numbers (see Table 2).

fects, we have computed the directional contrast (C_D) which is defined as the variation of the corrected signal as compared with the measured signal after atmospheric degradation. The directional contrast C_D is expressed as

$C_D = (\rho_1 - \rho_2) / (\rho^*_1 - \rho^*_2)$, where ρ_1 and ρ_2 are the corrected (exact) reflectances in two different viewing angles, and ρ^*_1 and ρ^*_2 are the measured apparent reflectances (Tanré *et al.*, 1979). Table 7 shows the maximum observed directional contrast deduced from the flight F1 data for several wavelengths and cover-types. Although the measurements were made at a low altitude, they are strongly affected by the atmospheric scattering processes, particularly in the shorter wavelengths. The two main mechanisms by which atmosphere perturbs the measurements are (1) increases in reflectances due to aerosol and molecular backscattering ($\Delta\rho < \Delta\rho^*$), the effect being accentuated at larger viewing angles, and (2) decreases in the ground reflectance

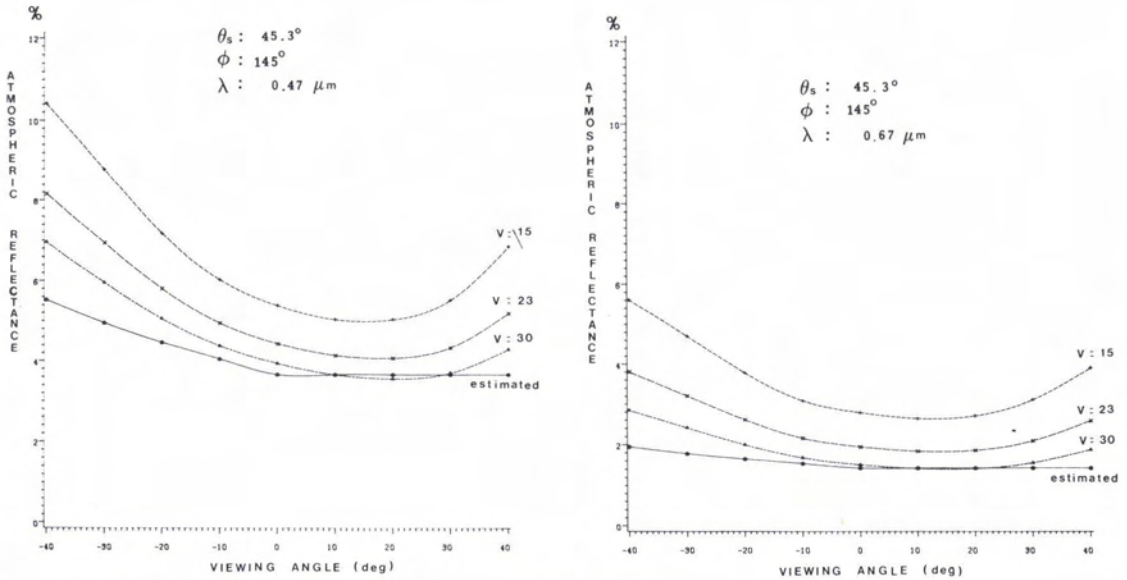

FIG. 7. Variation of the calculated intrinsic atmospheric reflectance with viewing angle for three visibilities (V expressed in km) and two wavebands, compared with the estimated atmospheric reflectance.

TABLE 7. DIRECTIONAL CONTRAST C_D (SEE TEXT) OF SEVERAL COVER-TYPE REFLECTANCES FROM F1 DATA AND FOR DIFFERENT WAVELENGTHS

λ (μm)	0.47	0.57	0.67	0.84
Grass	0.58	0.86	0.99	1.09
Corn	0.32	0.69	0.70	1.11
Pasture	0.94	0.77	0.82	1.10
Asphalt Road	0.64	0.68	0.92	1.09

contribution to the apparent measured reflectance ($\Delta\rho > \Delta\rho^*$) due to the transmission function.

THE BIDIRECTIONAL REFLECTANCE DISTRIBUTION FUNCTION

In order to compare the bidirectional properties of the ground reflectances, we have plotted $\rho(\theta_s,\theta_v,\phi)$ (Equation 1) as a function of the scattering angle (α) for all the targets of the flights (Figure 8). The scattering angle (α) reduces the number of angular variables to one and is computed according to

$$\cos\alpha = \cos\theta_s \cos\theta_v + \sin\theta_s \sin\theta_v \cos\phi.$$

Scattering angle values around 90° correspond to the specular zone, according to the range of the θ_s, θ_v, and ϕ values listed in Table 1, for the three flight lines used. Angles tending to 180° correspond to the antispecular or backscattering zone, and intermediate angles (135°) correspond to the scattering or diffuse zone.

The observed variations could also be well described by a quadratic regression. The deduced correlation coefficients computed for each cover-type and wavelength (Vincent, 1984) are somewhat smaller than those shown in Table 3 due to the combination of the three flights and R^2 being greater than 0.60.

The trends and magnitude of these results (shown for the red and near IR wavebands in Figure 8) suggest that $\rho(\alpha)$ is highly variable and depends on the optical properties of the surfaces, once the atmospheric effect has been eliminated. The optical properties of leaves, soil, and shadow, as well as their overall spatial arrangement within individual canopies, could explain the observed variations. For example, grass exhibits higher directional variations than does corn in the visible wavebands. The geometric structure of row corn increases the proportion of projected surface of soil in the field of view. In the near IR waveband, the soil reflectance is much lower than is the vegetative surface reflectance, in contrast to the visible bands (Figure 8). Consequently, the backscatter response of the soil in the IR has less effect on the directional reflectance as compared to the visible bands (Kimes *et al.*, 1984). Moreover, the shadows of the near IR region may not be as dark as those observed in the visible

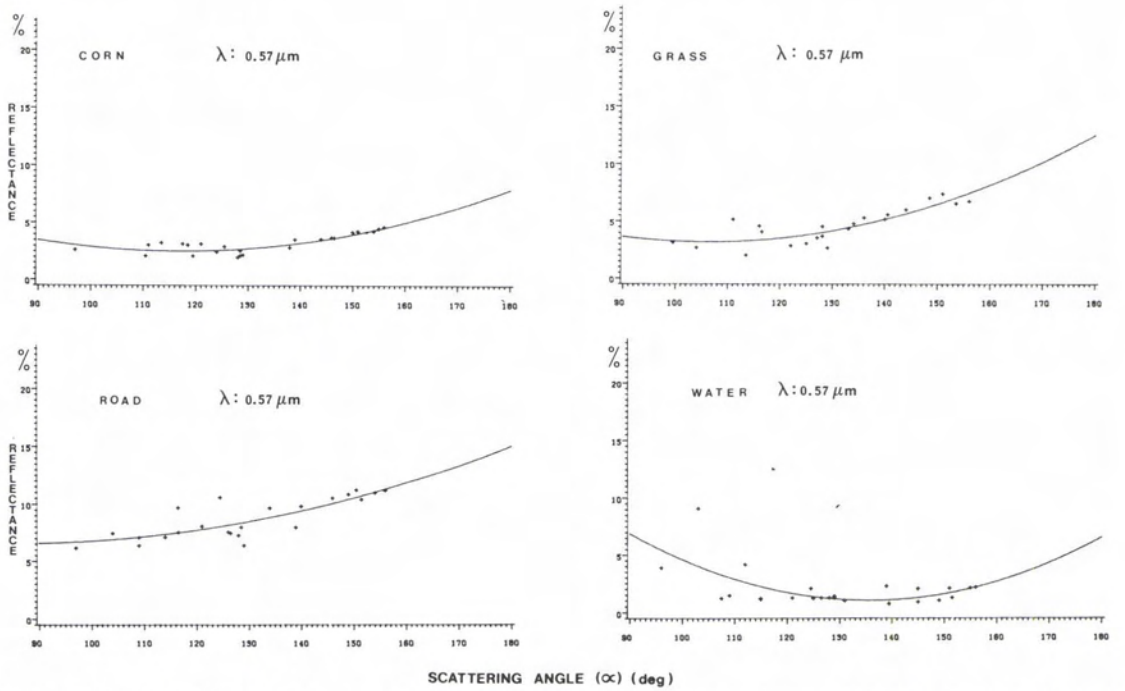

FIG. 8a. Bidirectional reflectance distribution function related to the scattering angle (α) (horizontal axis, in degrees) and for λ = 0.57 μm and for four cover-types. The curve correspond to the regression quadratic fit.

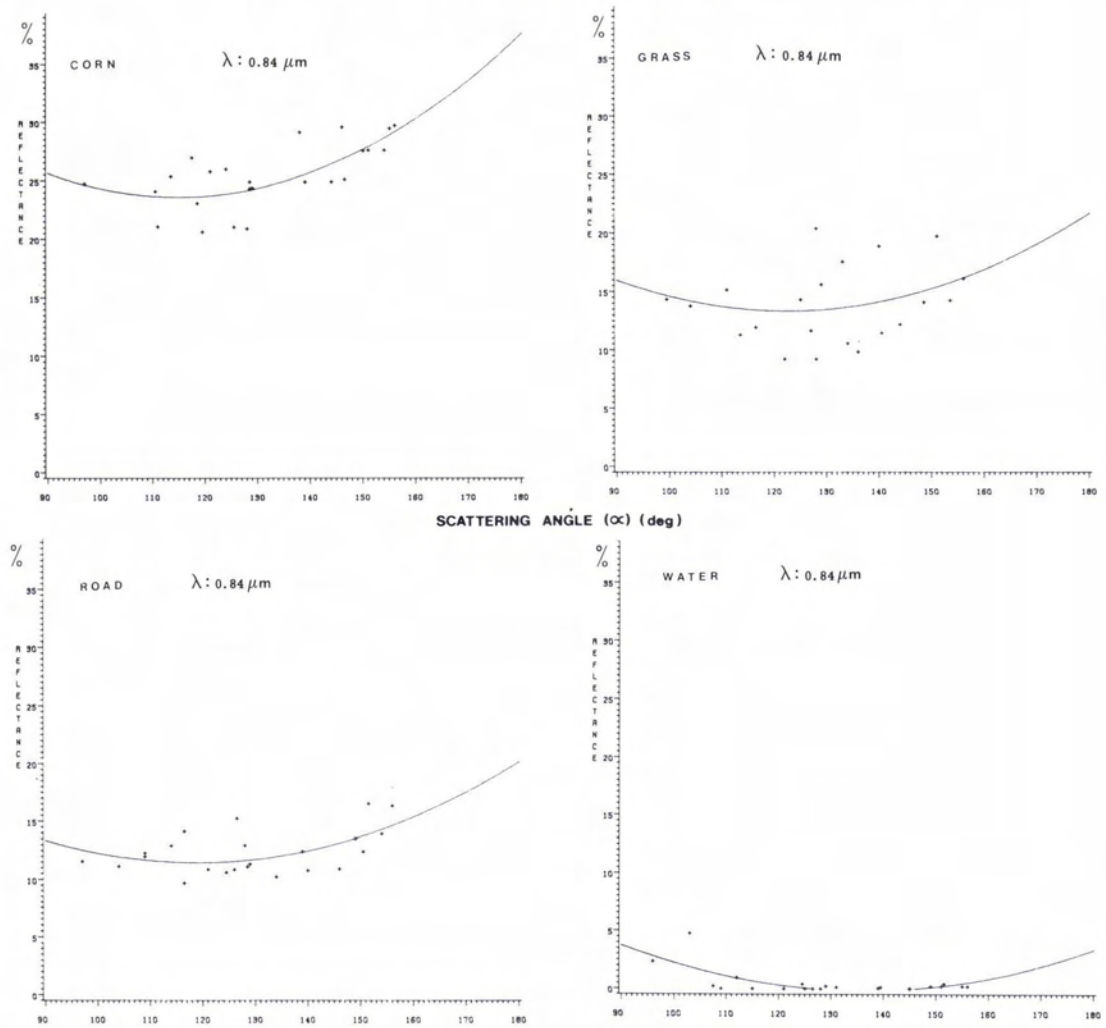

FIG. 8b. Same as Figure 8a but for $\lambda = 0.84$ μm. Horizontal axis: scattering angle (α) in degrees.

region due to low pigment absorption and multiple scattering in the canopy (Kollenkark *et al.*, 1981). This can be seen in the pasture reflectance variations, which are higher than those of the alfalfa.

DISCUSSION: SPATIAL CONTRAST

It was found that, for certain combinations of solar angles, marked differences in reflectance values occurred with large off-nadir viewing angles. These variations might be useful as an additional tool for target discrimination. Egbert and Ulaby (1972), Vanderbilt *et al.* (1980), and Guyot *et al.* (1981) have suggested the exploitation of such effects. The difference in contrast of targets can be seen on the spectral reflectivity curves plotted on Figure 9 for two sets of scattering angles. Figure 9a shows the spectral reflectance variations for α between 110° and 117°, which approximately corresponds to the nadir acquisition mode. Figure 9b shows the spectral reflectance variations for α between 150° and 156°, as would be the case for a sensor in an off-track pointing mode of about 35°. The spatial contrast $\{C_s = [(\rho_1 - \rho_2) / \rho_1] \times 100$ for $\lambda = 0.67$ μm, where ρ_1 and ρ_2 are the corrected directional reflectance for two neighboring targets, i.e. with the same viewing angle$\}$ is 1 percent in the nadir mode for the grass and green pasture, and 43 percent in the oblique mode. For pasture and alfalfa, C_s is found to be 2 percent and 19 percent, respectively, for the nadir and oblique modes at the same wavelength. On the other hand, for non-vegetative surfaces such as bare soil and asphalt road, C_s in the nadir mode (50 percent) is higher than in the oblique mode (2 percent).

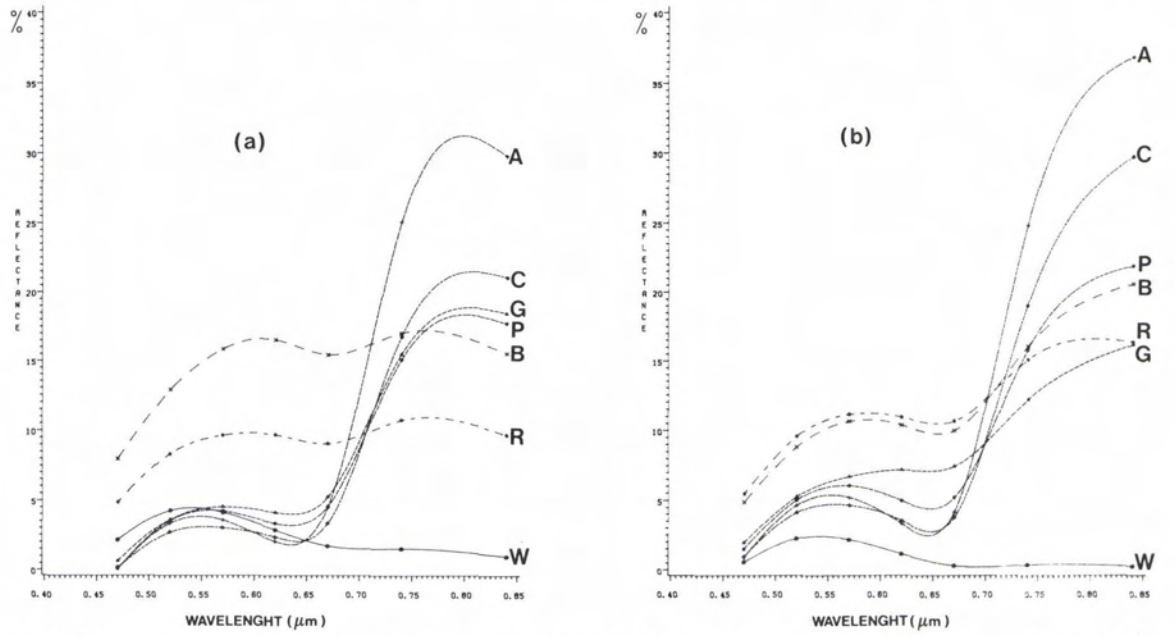

FIG. 9. Spectral variations of the bidirectional reflectance in the vertical mode (a) and the oblique mode (b), for seven covertypes. A: alfalfa, B: bare soil, C: corn, G: grass, P: pasture, R: road, W: water. The curves have been obtained with a smoothing spline function.

It can be concluded that the viewing angle dependence of reflectance might be used as an aid in detecting certain targets, particularly the vegetation canopies. This approach has fundamental implications for digital image analysis of data from the future HRV-SPOT sensor in the off-track pointing mode.

APPLICATION: A PRACTICAL METHOD FOR CORRECTING BIDIRECTIONAL REFLECTANCE VARIATIONS

Several authors have tried various correction procedures to improve the measurements obtained from space by means of mathematical modeling of the bidirectional reflectance distribution function (BRDF) (Hugli and Frei, 1983). The analytical BRDF can be calculated with the Minnaert equations (Hapke, 1963; Smith *et al.*, 1980), with the Duntley equations (Allen *et al.*, 1970; Suits, 1972), or by decomposition into two average angular reflectances as proposed by Tanré *et al.* (1983). The numerical BRDF can also be computed from an extensive set of ground measurements which cover the complete range of incidence and reflection parameters, as we have done in the previous section.

Several practical approaches have also been proposed for radiometric correction in remotely sensed images. Egbert (1977) and Shibata *et al.* (1981) discussed a correction method based on a simulated shading effect, including a digital elevation model over a mountainous terrain. Letts and Rochon (1980), Justice *et al.* (1981), Teillet *et al.* (1982) and Cavayas *et al.* (1983) analyze semi-empirical models for the slope-aspect correction of Landsat-MSS data.

However, for operational and routine use of remotely sensed images for continuous monitoring of crop conditions or for investigation over unknown and large areas, severe limitations are encountered with the above mentioned correction procedures. The first difficulty arises from the fact that the atmosphere and the surface are interacting, and in order to compute the absolute spectral reflectance characteristics, all the surface and atmospheric parameters should be known. Secondly, the use of digital terrain data is not always possible over large areas because it requires precise geometrically registered images, which can be a major limitation for airborne data or for very wide scan images. Thus, some *a priori* knowledge of the analyzed surfaces is needed, and the use of a bidirectional reflectance distribution model could significantly increase the cost and time of image processing.

In order to avoid these problems, a correction procedure is needed which calculates relative angular corrections to bidirectional reflectance measurements independently of the details of surface characteristics.

SPECTRAL RATIO IMAGING METHOD

The simplest method for correcting radiance variations across a sensor scan line is the spectral ratio method. Several combinations of ratioing techniques, such as a simple division of adjacent chan-

nels (Cranes, 1971; Barnsley, 1983) or the ratio of the near IR and red difference to their sum (e.g., the vegetative index (Holben and Fraser, 1983; Piwinski *et al.*, 1983; Staenz *et al.*, 1983)), have been proposed to compensate for space data variations with viewing angle. These techniques have also commonly been used to reduce the topographic effect (Vincent, 1973; Holben and Justice, 1981).

The variations of single band ratios (channel ratios 4/3, 5/4, 7/6, and 9/8) with the viewing angle were analyzed. The scan-angle contrast is significantly reduced. The polynomial regression analysis indicates that the behavior of the channel ratios with viewing angle are well described by a straight line with a slope close to zero (Vincent, 1984). Thus, the bidirectional effect is very similar for two adjacent and narrow wavebands. As the ratio tends to significantly remove the viewing angle effects, the directional reflectance function could be defined, in effect, as a multiplicative noise.

However, for larger band widths, the ratio values still exhibit significant variations with changing viewing angle, as shown by Piwinski *et al.* (1983) on AVHRR wavebands and by Barnsley (1983). Furthermore, even if a correction for scan angle effect can be made by the ratioing technique, retrieval of the spectral reflectance from the ratio is not possible.

Normalization Method

Several approaches have been used to correct for the viewing angle effects based on the normalization of measured radiances by the mean radiance variation factor. We first generate the curve of the mean raw digital radiance values $[P_x(i)]$ versus the pixel position (i) related to the viewing angle. The observed variations are described by a polynomial fit of the form $P_x(i) = a + b(i) + c(i)^2$.

The first correction procedure (CP1) consists of substracting the generated curve from the measured radiances. The corrected radiance X'_i at pixel position (i) is then calculated from the equation:

$$X'_i = X_i - (P_x(i) - P'(x)) \qquad \text{(CP1)}$$

where X_i is the measured radiance, $P_x(i)$ is the corresponding mean raw radiance value, and P'(x) is the mean corrected radiance value. $P'(x)$ is equal to the minimum value of $P_x(i)$, which occurs at the position where $X'_i = X_i$ (i.e., at the nadir). A similar approach was used by Brown *et al.* (1982), but this procedure has certain deficiences. One is that the mean regression curve $P_x(i)$ can differ greatly from the variation curves of certain surface radiances with respect to viewing angle. We have shown that the viewing angle effects on various cover-type radiances are significantly different from each other. Hence, correction procedure 1 will only be useful in digital image processing for homogeneous areas. In this case, $P_x(i)$ will be defined by the variation curve of the surface.

In a second correction procedure (CP2), the measured radiances are normalized by the polynomial function $P_x(i)$. The corrected radiance X_i is calculated from the equation

$$X'_i = [X_i / P_x(i)]\, P'(x). \qquad \text{(CP2)}$$

If we consider the corrected radiances (X'_i) and the raw radiances (X_i) as two normal random distributions defined by the mean values $P'(x)$ and $P_x(i)$, respectively, then we equalize the centered variables with CP1: i.e.,

$$[X'_i - P'(x)] = [X_i - P_x(i)],$$

and we equalize the normalized variables with CP2: i.e.,

$$[X'_i / P'(x)] = [X_i / P_x(i)].$$

If $P'(\sigma)$ and $P_\sigma(i)$ are the mean standard deviations of the corrected radiance distribution and the original radiance distribution, respectively, we show that the principle of the equalization of the standardized variables

$$\frac{X'_i - P'(x)}{P'(\sigma)} = \frac{X_i - P_x(i)}{P_\sigma(i)} \qquad (2)$$

is approximately equivalent to CP2. This is due to the fact that the variations of the mean values and the standard deviation with the viewing angle are exactly the same: i.e.,

$$P_x(i) / P_\sigma(i) = \text{const.}$$

From Equation 2, we then deduce that

$$X'_i = A[X_i / P_x(i)] - B \qquad (3)$$

where $A = P'(\sigma)$ and $B = P'(\sigma)\,[P_x(i)P_\sigma(i)] + P'(x)$ are constants. Equation 3 is similar to CP2. The relation (Equation 2), based on a statistical approach, may be used as another correction procedure (G. Rochon, personal communication). However, we have only considered here CP2, which is similar and simpler.

Two other correction procedures have also been performed to correct the viewing angle effect. They are based on the normalization of the raw radiance values which have been corrected for the atmospheric path radiance variation. The corrected radiance X'_i is expressed by

$$X'_i = \frac{[X_i - U_i(i)]\, P'(x)}{P_x(i)} \qquad \text{(CP3 and 4)}$$

$$\text{where } U(i) = L_p\,[f(i)/f_o(i)] \qquad \text{(CP3)}$$

$$\text{or } U(i) = L_p - [f(i) - f_o(i)] \qquad \text{(CP4)}$$

L_ρ is the nadir atmospheric path radiance, $f(i)$ is the variation function of the path radiance with viewing angle, and $f_o(i)$ the minimum value of $f(i)$.

TABLE 8. SCAN-ANGLE CONTRAST (%) COMPUTED BEFORE CORRECTION (CPO) AND AFTER CORRECTION PROCEDURES 1 AND 2 (CP1 AND CP2)

Surfaces	CP	λ (μm) 0.47	0.57	0.67	0.84	Mean Values
Grass	0	78	73	67	79	74
	1	26	34	39	58	39
	2	25	32	34	24	29
Alfalfa	0	67	48	14	28	39
	1	37	36	41	19	33
	2	21	33	32	30	29
Corn	0	63	55	29	38	46
	1	36	28	38	19	30
	2	20	27	27	34	27
Pasture	0	72	53	27	63	54
	1	27	30	56	40	38
	2	20	27	29	16	23
Mean	0	70	57	40	52	55
	1	32	32	44	34	36
	2	22	22	31	26	27

RESULTS AND ERROR ANALYSIS

The four procedures were used to correct the directional reflectance effects in the airborne images, and their efficiency was analyzed by comparing the radiance variation curves, regression analyses, and supervised classifications of the original and corrected data sets. The scan-angle contrast of the vegetal cover-types corrected with CP1 and CP2 are shown in Table 8. Both procedures significantly reduced the scan-angle contrast, though CP2 appears to be more effective (mean scan-angle contrast 27 percent), as well as removing major radiometric inhomogeneities in the image (Figure 1). However, the extreme specular variations are not corrected. Both CP3 and CP4 give results similar to CP2 but with a better contrast in the image.

We have tested the correction procedures with scattergram techniques by comparing both F1-F4 and F2-F5 data sets. The large overlap area of the F1 image was registered to the adjacent parallel F4 image. In the overlap side of the F1 image, F1 radiances do not present directional effects and can thus be used as reference data, while the corresponding F4 radiances exhibit high backscattered signals. There is a good correlation ($R^2 = 0.7$) between the F1 data and the corrected (F4) data. CP2, with a regression line slope close to 1, significantly reduces the intrinsic source of radiance variation. CP3 and CP4 introduce more variation into the data at low gray levels due to the substracted path radiance. Similar results are deduced from the scattergram analysis of F2-F5, which have a different illumination geometry.

Based on the first two tests, it is concluded that the correction procedures significantly remove the viewing angle effects, particularly the normalization procedure 2. These simple procedures are useful for current image processing techniques employed in vegetation studies or monitoring of crop conditions. These procedures could also be applied to making digital image mosaïcs by adjusting the normalized average gray level of two adjacent images.

Finally, the results of supervised classifications of the raw and corrected images were compared to evaluate the effects of the correction procedures on the classification accuracy. The Baysian maximum likelihood classification algorithm (Dipix, 1983) was used with four input channels (channels 3, 5, 7, and 9, Table 2) and eight supervised training areas, including the seven themes previously described and a forest area, thus incorporating all the different land-use categories present in the survey area. The training areas were chosen from the central part of the flight F1 image so as to avoid directional reflectance effects. Table 9 gives a summary of the results obtained with a classification threshold of 95 percent for the F1 data set. The gain in accuracy is readily apparent if one compares the percentage of misclassified pixels for each correction procedure. CP2, CP3, and CP4 improve the discrimination and classification accuracy of the eight cover types. On the average, 38 percent more pixels were correctly classified with CP2 than without correction.

CONCLUSION

The results presented in this study indicate that there is an important variation in detected radiance with increasing off-nadir viewing angle. The observed variations with viewing angle are not usually symmetrical about the nadir, are accentuated with increasing solar zenith angle, and are maximized when the scan direction is parallel to the incoming solar radiation. The illumination and viewing-geometry effects were found to be related to cover

TABLE 9. CLASSIFICATION ACCURACY EXPRESSED IN PERCENT FOR EACH CORRECTION PROCEDURE

Classes	Without Correction	Correction Procedure			
		1	2	3	4
Well Classified Pixels (%)					
Water	92	92	91	91	91
Grass	0	23	17	10	17
Alfalfa	0	17	20	19	10
Corn	0	22	36	14	5
Pasture	0	39	47	59	48
Asphalt Road	14	50	57	12	16
Bare Soil	7	31	81	93	90
Forest	5	81	92	94	94
Misclassified Pixels (%)	43	24	15	10	10
Total Well Classified Pixels (%)	28	51	66	64	60

type and, in particular, to variations in the proportions of illuminated and shadowed leaf components. The directional factor function is characteristic of each type of canopy. These surface-radiation interactions also vary with wavelength. When these variations are properly understood and used to advantage, they increase separability or spatial contrast of targets.

Simple and practical methods for correcting bidirectional reflectance variations have been proposed, which remove radiometric inhomogeneities in images recorded with wide scan angles. The procedures also allow us to compare directly images recorded in vertical and oblique modes.

ACKNOWLEDGMENTS

We are very grateful to G. Rochon, P. M. Teillet, D. Tanré, A. Podaire, P. Y. Deschamps, and Q. H. J. Gwyn for helpful criticism and discussions. G. Saint and J. Perbos at CNES/LERTS also provided technical assistance for the atmospheric correction software. Ground truth facilities were provided by the Experimental Farm of Agriculture Canada (Lennoxville, Québec) and the "Centre de Recherche en Écologie de Montréal" (Québec).

The study was supported by Natural Sciences and Engineering Research Council of Canada (Grant A 8643), Fonds FCAR, Québec (Grant EQ 102), the Department of Agriculture Québec (Grant CRSAQ S-82-954), and Agriculture Canada (Grant 83035).

REFERENCES

Allen, W. A., T. V. Gayle, and A. J. Richardson, 1970. Plant Canopy Irradiance Specified by the Duntley Equation. *J. of Optical Society of America*, Vol. 60, No. 3, pp. 372-376.

Barnsley, M. J., 1983. The Implications of View Angle Effects on the Use of Multispectral Data for Vegetation Studies. *Proc. of the Int. Conf. on Remote Sensing for Rangeland Monitoring and Management*, Bedford, United Kingdom, pp. 166-177.

Bonhomme, R., G. Guyot, and J. Riom, 1978. Relations existant entre la réflectance d'un couvert végétal et sa structure, la hauteur du soleil et l'angle de visée. Perspectives de modélisation. *Proc. of an Int. Conf. on Earth Observation from Space and Management of Planetary Resources*, Toulouse, France, pp. 319-325.

Brown, R. J., M. Bernier, and G. Fedosejevs, 1982. Geometrical and Atmospheric Considerations of NOAA AVHRR Imagery. *Proc. of the 8th Symp. on Machine Processing of Remotely Sensed Data*, West Lafayette, pp. 374-381.

Cavayas, F., G. Rochon, and P. Teillet, 1983. Estimation des réflectances bidirectionnelles par analyse des images Landsat: Problèmes et possibilités de solutions. *Comptes rendus du 8e Symp. Canadien de télédétection*, Montréal, Canada, pp. 645-664.

Chevrel, M., M. Courtois, and G. Weill, 1981. The SPOT Satellite Remote Sensing Mission. *Photogrammetric Engineering and Remote Sensing*, Vol. 47, No. 3, pp. 1163-1171.

Crane, R. B., 1971. Prepocessing Techniques to Reduce Atmospheric and Sensor Variability in Multispectral Scanner Data. *Proc. of the 7th Int. Symp. on Remote Sensing of Environment*, Ann Arbor, Michigan, pp. 1345-1355.

D'Arodes, M. C., A. Podaire, and G. Saint, 1983. Analyse des effets directionnels sur la végétation et les sols. *Comptes rendus du 2e Coll. Int. sur les Signatures Spectrales d'Objets en Télédétection*, Bordeaux, France, pp. 159-170.

Dave, J. V., 1980. Effects of atmospheric conditions on remote sensing of a surface nonhomogeneity. *Photogrammetric Engineering and Remote Sensing*, Vol. 46, No. 9, pp. 1173-1180.

Deschamps, P. Y., M. Herman, and D. Tanré, 1981. Influence de l'atmosphère en télédétection des ressources terrestres. Modélisation et possibilités de corrections. *ISP: Signatures Spectrales d'Objets en Télédétection*, Avignon, France, pp. 543-558.

Dipix, 1983. *General Technical Description of the ARIES-II Digital Image Analysis System*. Dipix System Limited, Ottawa, Canada.

Duggin, M. J., 1977. Likely Effects of Solar Elevation on the Quantitative Changes in Vegetation with Maturity Using Sequential Landsat Imagery. *Applied Optics*, Vol. 16, pp. 521-523.

Eaton, F. D., and I. Dirmhin, 1979. Reflected Irradiance Indicatrices of Natural Surfaces and Their Effect on Albedo. *Applied Optics*, Vol. 18, No. 7, pp. 994-1008.

Egbert, D. D., 1977. A Practical Method for Correcting Bidirectional Reflectance Variations. *Proc. of the Symp. on Machine Processing of Remotely Sensed Data*, West Lafayette, pp. 178-188.

Egbert, D. D., and F. T. Ulaby, 1972. Effect of Angles on Reflectivity. *Photogrammetric Engineering*, Vol. 38, No. 6, pp. 556-564.

Guyot, G., 1980. Analyses of Factors Acting on the Variability of Spectral Signatures of Natural Surfaces. *Int. Archives of Photo.*, Vol. 22, section P7, pp. 382-393.

Hapke, B. W., 1963. A Theoretical Photogrammetric Function for the Lunar Surface. *J. of Geophysical Research*, Vol. 68, No. 15, pp. 4571-4586.

Holben, B. N., and C. O. Justice, 1981. An Examination of Spectral Band Ratioing to Reduce the Topographic Effect on Remotely Sensed Data. *Int. J. of Remote Sensing*, Vol. 2, No. 2, pp. 115-133.

Holben, B. N., and R. S. Fraser, 1983. Effects of Atmosphere and View and Illumination Geometry on Visible and Near Infrared Radiance Data from the Advanced Very High Resolution Radiometer (AVHRR). *Proc. of the 17th Int. Symp. on Remote Sensing of Environment*, Ann Arbor, Michigan, pp. 1091-1100.

Hugli, H., and W. Frei, 1983. Understanding Anisotropic Reflectance in Mountainous Terrain. *Photogrammetric Engineering and Remote Sensing*, Vol. 49, No. 5, pp. 671-683.

Jackson, R. D., R. J. Reginato, P. J. Pinter, Jr, and S. B. Idso, 1979. Plant Canopy Information Extraction from Composite Scene Reflectance of Row Crops. *Applied Optics*, Vol. 18, pp. 3775.

Justice, C. O., S. W. Wharton, and B. N. Holben, 1981. Application of Digital Terrain Data to Quantify and Reduce the Topographic Effect on Landsat Data. *Int. J. of Remote Sensing*, Vol. 2, No. 3, pp. 213-230.

Kaufman, Y. J., and R. S. Fraser, 1983. Different Atmospheric Effects in Remote Sensing of Uniform and Nonuniform Surfaces. *Adv. Space Res.*, Vol. 2, No. 5, pp. 147-155.

Kimes, D. S., J. A. Smith, and K. J. Ranson, 1980. Vegetation Reflectance Measurements as a Function of Solar Zenith Angle. *Photogrammetric Engineering and Remote Sensing*, Vol. 46, No. 12, pp. 1563-1573.

Kimes, D. S., W. W. Newcomb, and J. B. Schutt, 1984. Directional Reflectance Factor Distributions of a Cotton Row Crop. *Int. J. of Remote Sensing*, Vol. 5, No. 2, pp. 263-277.

Kollenkark, J. C., V. C. Vanderbilt, C. S. T. Daughtry, and M. E. Bauer, 1981. Canopy Reflectance as Influenced by Solar Illumination Angle. *AGRISTARS*, SR-P1-04039, NAS9-15466, 21 p.

Kriebel, K. T., 1978. Measured Spectral Bidirectional Reflection Properties of Four Vegetated Surfaces. *Applied Optics*, Vol. 17, No. 2, pp. 253-258.

Letts, P. J., and G. Rochon, 1980. Generation and Use of Digital Elevation Data for Large Areas. *Proc. of the 6th Canadian Symp. on Remote Sensing*, Halifax, Canada, pp. 598-602.

McColl, W., 1982. *Universal Format CCRS Airborne MSS/MEIS Imagery CCT*. Technical Memorandum, DPD-TM-79-082A. CCRS, Ottawa, Canada.

Piech, K. R., and J. R. Schott, 1974. Atmospheric Corrections for Satellite Water Quality Studies. *Proc. of S.P.I.E.*, Vol. 51, pp. 84-100.

Piwinski, D. J., L. B. Schoch, M. J. Duggin, V. Whitehead, and E. Ryland, 1983. Dependance of NOAA-AVHRR Recorded Radiance of Scan Angle, Atmospheric Turbity and Unresolved Cloud. *Proc. of the 17th Int. Symp. on Remote Sensing of Environment*, Ann Arbor, Michigan.

Rao, V. R., E. J. Brach, and A. R. Mack, 1979. Bidirectional Reflectance of Crops and the Soil Contribution. *Remote Sensing of Environment*, Vol. 8, pp. 115-125.

Shibata, T., W. Frei, and M. Sutton, 1981. Digital Correction of Solar Illumination and Viewing Angle Artifacts in Remotely Sensed Images. *Proc. of the Symp. on Machine Processing of Remotely Sensed Data*, West Lafayette, pp. 169-177.

Slater, P. N., 1980. *Remote Sensing: Optics and Optical Systems*. Addison-Wesley, Reading, Mass.

Smith, J. A., Tzeu Lie Lin, and K. J. Ranson, 1980. The Lambertian Assumption and Landsat Data. *Photogrammetric Engineering and Remote Sensing*, Vol. 46, No. 9, pp. 1183-1189.

Staenz, K., F. J. Ahern, and R. J. Brown, 1981. The Influence of Illumination and Viewing Geometry on the Reflectance Factor of Agricultural Targets. *Proc. of the 15th Int. Symp. on Remote Sensing of Environment*, Ann Arbor, Michigan, pp. 867-882.

Staenz, K., R. J. Brown, and P. M. Teillet, 1983. Influence of the Viewing Geometry on Vegetation Measures. *Proc. of the 8th Canadian Symp. on Remote Sensing*, Montréal, Canada, pp. 5-12.

Suits, G. H., 1972. The Calculation of the Directional Reflectance of a Vegetative Canopy. *Remote Sensing of Environment*, Vol. 2, pp. 117-125.

Tanré, D., M. Herman, P. Y. Deschamps, and A. De Leffe, 1979. Atmospheric Modeling for Space Measurements of Ground Reflectances, Including Bidirectional Properties. *Applied Optics*, Vol. 18, No. 21, pp. 3587-3594.

Tanré, D., M. Herman, and P. Y. Deschamps, 1981. Influence of the Background Contribution upon Space Measurements of Ground Reflectances. *Applied Optics*, Vol. 20, pp. 3676-3684.

———, 1983. Influence of the Atmosphere on Space Measurements of Directional Properties. *Applied Optics*, Vol. 21, pp. 733-741.

Teillet, P. M., B. Guindon, and D. G. Goodenough, 1982. On the Slope-Aspect Correction of Multispectral Scanner Data. *Canadian J. of Remote Sensing*, Vol. 8, No. 2, pp. 84-106.

Turner, R. E., and M. M. Spencer, 1972. Atmospheric Model for Correcting the Space Craft Data. *Proc. of the 8th Int. Symp. on Remote Sensing of Environment*, Ann Arbor, Michigan, pp. 895-934.

Vanderbilt, V. C., B. F. Robinson, L. L. Biehl, M. E. Bauer, and A. S. Vanderbilt, 1981. *Simulated Response of a Multispectral Scanner over Wheat as a Function of Wavelength and View Illumination Direction*. Technical Report, SR-P1-04202, NA9-15466, LARS 071580, 11 p.

Vincent, R. K., 1973. Spectral Ratio Imaging Methods for Geological Remote Sensing from Aircraft and Satellites. *Proc. of Symp. on Management and Utilisation*

of Remotely Sensed Data, A.S.P., Sioux Falls, S.D., pp. 377-397.

Vincent, P., F. J. Bonn, and P. Gangloff, 1983. Simulations SPOT et Landsat-4: Généralisation des données d'inventaire biophysique de la MRC du Haut Saint-Laurent, analyse préliminaire. *Comptes rendus du 8e Symp. Canadien de télédétection*, Montréal, Canada, pp. 507-518.

Vincent, P., 1984. *Évaluation des réflectances bidirectionnelles par télédétection aéroportée et méthodes de correction*. M. S. Thesis, Laboratoire de Télédétection, Dépt. de Géographie, Université de Sherbrooke, Sherbrooke, Canada, 137 p.

Zwick, H., W. D. McColl, and H. R. Edel, 1980. The CCRS DS1260 Airborne Multispectral scanner (MSS). *Proc. of the 6th Canadian Symp. on Remote Sensing*, Halifax, Canada, pp. 643-648.

(Received 26 November 1984; revised and accepted 2 April 1985)

International Society for Photogrammetry and Remote Sensing
Commission III

CALL FOR PAPERS

International Symposium
From Analytical to Digital

Lappia-House, Rovaniemi, Finland
19-22 August 1986

This Inter-Congress Symposium of Commission III of the International Society for Photogrammetry and Remote Sensing is dedicated to the late Dr. K. G. Löfstrom, a pioneer of photogrammetry in Finland. Technical Sessions dealing with the subjects of the Working Groups of Commission III are as follows:

WG III/1	Accuracy Aspects of Combined Point Determination
WG III/2	On-Line Photogrammetric Triangulation
WG III/3	Digital Terrain Models
WG III/4	Mathematical Aspects of Image Analysis and Pattern Recognition
WG III/IV	Digital Technology for the Integration of Photogrammetric and Remote Sensing Data with Land/Geographic Information Systems

Those wishing to present a paper must submit an extensive abstract by *15 February 1986* to

Symposium of Commission III
Institute of Photogrammetry
Helsinki University of Technology
02150 Espoo, Finland
Phone: Int. +358 0 451 2523 or 2524